Chinese Journal of Aeronautics, (2015),28(2): 600–608

Chinese Society of Aeronautics and Astronautics
& Beihang University

Chinese Journal of Aeronautics

cja@buaa.edu.cn
www.sciencedirect.com

Effects of cerium salts on corrosion behaviors of Si–Zr hybrid sol–gel coatings

Yu Mei *, Liu Yuxing, Liu Jianhua, Li Songmei, Xue Bing, Zhang You, Yin Xiaolin

School of Materials Science and Engineering, Beihang University, Beijing 100191, China

Received 29 August 2014; revised 24 October 2014; accepted 20 November 2014
Available online 21 February 2015

KEYWORDS

Cerium salts;
Corrosion resistance;
Hybrid coating;
Inhibitor

Abstract The present work examines the effects of cerium salts on corrosion behaviors of Si–Zr hybrid sol–gel coatings. The Si–Zr hybrid sol–gel coatings on a 2A12 aluminum substrate were prepared through hydrolysis and condensation of glycidoxypropyl-trimethoxy-silane (GTMS) and zirconium(IV) *n*-propoxide (TPOZ). Used as inhibitors for corrosion, three types of cerium salts ($Ce(NO_3)_3$, $CeCl_3$, and $Ce(CH_3COO)_3$) were doped into the sol–gel coatings. Fourier transform infrared (FTIR) and scanning electron microscopy (SEM) were employed to investigate the structures and morphologies of various coatings, and the corrosion resistances of the coatings were evaluated by electrochemical methods and neutral salt spray tests. Experimental results indicate that the addition of cerium salts can hinder the process of corrosion due to their self-healing abilities. Furthermore, the sol–gel coating doped with $Ce(CH_3COO)_3$ has the best corrosion resistance because of the promotions of hydrolysis and condensation provided by CH_3COO^-.

1. Introduction

Aluminum alloys have been extensively used in many fields including aeronautics, building, and automotive industries. Thereinto, alloy 2A12 is paid special attention with its remarkable mechanical strength.[1] However, the heterogeneous microstructure makes 2A12 highly susceptible to various kinds of atmospheric corrosion such as pitting corrosion, intergranular corrosion, and even exfoliation corrosion.[2] Thus, the corrosion behavior of 2A12 has become a major concern when exposed to environmental conditions which need to be prevented or retarded by applying environmentally friendly coatings. As a viable alternative to chromates, sol–gel-based coatings have been deposited on 2A12 and exhibit good barrier effects to severe environments.[3–5]

Si–Zr-based organic–inorganic hybrid sol–gel coatings have been widely studied for corrosion protection of various metals.[6–8] The hybrid coatings are proven to possess good adhesion with substrates, along with stable corrosion protection properties.[8–10] Moreover, mixed SiO_2 and ZrO_2 oxide layers deposited on aluminum alloy via the sol–gel technique increase the "bridge" effect between organic and inorganic phases.[8] The

* Corresponding author. Tel.: +86 10 82317103.
E-mail addresses: yumei@buaa.edu.cn (M. Yu), liuyx@mse.buaa.edu.cn (Y. Liu).
Peer review under responsibility of Editorial Committee of CJA.

Production and hosting by Elsevier

http://dx.doi.org/10.1016/j.cja.2015.01.011
1000-9361

presence of the organic part makes the sol–gel network more flexible and less prone to cracking during the drying process, while the inorganic part increases the hardness and hydrophilic property of the coatings.[11] However, due to the lack of a self-healing property, the sol–gel coatings cannot stop the development of a corrosion process when defects appear. To solve this problem, corrosion inhibitors have been introduced into sol–gel coatings.

To date, many corrosion inhibitors have been doped to sol–gel coatings to increase the corrosion resistances of the coatings.[12–16] Among these inhibitors, cerium salts are considered to be a good type of corrosion inhibitors.[17–23] Corrosion protection offered by cerium-containing coatings is mainly achieved by the obstruction of the cathodic oxygen reduction reaction.[24] Ref.[25] proposed that cerium ions could substitute some of the Si atoms in the coatings, leading to the formation of a modified Si–O–Ce network. In addition, it was reported that a combination of different inhibiting species such as rare earth elements with organic acid groups could provide a synergistic inhibition effect,[26,27] and consequently confer a superior corrosion inhibition for alloys. Cerium phosphates,[28] cerium cinnamate,[29] and cerium silicate[30] were tested as inhibitors and exhibited promising corrosion resistances. However, data are still scarce about the inhibitive behaviors of cerium salts with organic acid group and inorganic anion. Meanwhile, it would be interesting to compare and discuss the effects of various cerium salts when incorporated in hybrid sol–gel coatings. To this end, three types of cerium salts ($Ce(NO_3)_3$, $CeCl_3$, and $Ce(CH_3COO)_3$) used as inhibitors for the corrosion process were doped into Si–Zr hybrid coatings. Tests of scanning electron microscopy (SEM), Fourier transform infrared (FTIR), immersion coupled with electrochemical methods and neutral salt spray were conducted to evaluate and compare the performances of the coatings.

2. Experimental

2.1. Preparation of the substrate

The nominal composition of 2A12 aluminum alloy is given in Table 1. Before deposition, the alloy was cut into rectangular panel samples with a dimension of 40 mm × 20 mm × 2 mm. Then the samples were mechanically abraded with abrasive papers up to grit #600, and cleaned and etched according to the following procedure: (1) degreasing in alkaline cleaner at 50 °C for 1–2 min, (2) alkaline cleaning in 50 $g{\cdot}L^{-1}$ NaOH solution at 60 °C for 30 s, and (3) acid etching in acid aqueous (CrO_3, 50 $g{\cdot}L^{-1}$; HNO_3, ρ = 1.42 $g{\cdot}mL^{-1}$, 100 $g{\cdot}L^{-1}$; HF, 40 wt%, 10 $g{\cdot}L^{-1}$) to remove oxide at room temperature. Finally, the samples were rinsed in water and dried in air.

Table 1 Nominal composition of 2A12 aluminum alloy.

Element	Concentration (wt%)
Cu	3.8–4.9
Mg	1.2–1.8
Mn	0.3–0.9
Zn	0.25
Si	0.5
Fe	0.5
Al	Balance

2.2. Preparation of the coatings

The Si–Zr organic/inorganic hybrid coatings were prepared by the sol–gel technology. Concurrently, two separate sols, a Si sol and a Zr sol, were formulated. The Si sol was prepared by mixing glycidoxypropyl-trimethoxy-silane (GTMS, analytical, Nanjing Capatue Chemical Co., Ltd, China) with ethanol of equal volume. Distilled water was dropwise added to enable hydrolysis of GTMS while continuously stirring the solution, and the molar quantity of the distilled water was one third of ethanol. For the Zr sol, Zirconium(IV) *n*-propoxide (TPOZ, 70% w/w in *n*-propanol, Alfa Aesar), ethyl acetoacetate, and ethanol were used as the source of hydrolysable zirconium, the catalyst, and the solvent, respectively. TPOZ was stirred with ethanol and ethyl acetoacetate in a volume ratio of 8:12:3. Both of the two solutions were stirred for 1 h in sealed beakers, and then the Zr sol was gently added into the Si sol with stirring. The molar ratio of Si to Zr in the mixed solution was 3:1. Afterwards, the mixed solution was sealed and kept on stirring for 3 h. Finally, three different types of cerium salts ($Ce(NO_3)_3$, $CeCl_3$, $Ce(CH_3COO)_3$) were added respectively, followed by stirring for 30 min. The mixed solution had a final concentration of cerium salts of 0.01 mol/L.

The coatings were deposited on the aluminum alloy samples by dip-coating with a withdraw speed of 10 $cm{\cdot}min^{-1}$ for two times. The time of each immersion into the solution was 5 min. Between the two immersions, the samples were dried in air for 15 min. After the second immersion, the samples were cured at 60 °C for 3 h, 90 °C for 1 h, and 120 °C for 0.5 h in an oven.

2.3. Characterizations

Sol–gel hybrid coatings with different types of cerium salt were analyzed by using an SEM (Apollo 300, Cam Scan, Britain) to investigate the morphologies of the coatings. Viscosity measurements of sols doped with different types of cerium salts were performed using a digital rotary viscometer (NDJ-5S, China) at 25 °C, with a measurement range from 1 mPa·s to 10^5 mPa·s.

Electrochemical tests were carried out by using an Advanced Electrochemical System (PARSTAT 2273, Princeton, USA). A three-electrode cell was employed, consisting of a saturated calomel reference electrode (SCE), a platinum foil as a counter electrode, and a coated sample as a working electrode with a surface area of 1 cm^2. In order to verify a "self-healing" property promoted by cerium ions, as well as to understand the mechanism of ongoing corrosion in different stages of the immersion period, the slow release of chloridion is desirable. Therefore, 0.05 mol/L NaCl solution was used as the test solution. Electrochemical impedance spectroscopy (EIS) measurements were conducted with an AC excitation amplitude of 10 mV at open circuit potential (OCP). The frequency range was from 100 kHz to 10 mHz with 50 data points. Before each measurement, the coated samples were immersed into the NaCl solution for 30 min until they reached a steady state. All the spectra were recorded at OCP. Several equivalent circuits were proposed to fit the EIS data and extract related electrochemical parameters by using the ZSimpWin software. In order to ensure reproducibility of the measurements, the samples were tested in triplicate.

The corrosion resistances of the coated samples were examined by putting them into a salt spray chamber (WYX/Q-250, YaShiLin, China). The spray solution was 5 wt% NaCl solution (pH 6.5–7.2). The temperature was kept at 35 °C, and the angle of the tested surface was set at 20°.

FTIR measurements of the coated samples were performed on a Thermo Nicolet Nexus 470 Fourier transform spectrometer. The spectra were averages of 32 scans, and the range of the FTIR spectra was about 500–4000 cm^{-1}.

3. Results and discussion

3.1. Morphologies of coatings

The SEM images of the cross sections of various coatings are shown in Fig. 1. It can be seen that the coatings are tightly adhered to the surface of the 2A12 aluminum substrate, and no obviously separated layer is detected within the coatings. This phenomenon indicates that the double dip-coating does not influence the adherence between the two layers. The thicknesses of the coatings doped with cerium salts ($Ce(NO_3)_3$ (2.334 μm), $CeCl_3$ (2.456 μm), and $Ce(CH_3COO)_3$ (2.484 μm)) are significantly higher than that of the undoped coating (1.856 μm). This phenomenon is closely related to the viscosities of the sols, which are shown in Table 2. It can be observed that the viscosities of the Ce-doped sols are much higher than that of the undoped one. Ref.[31] has shown that the addition of a cerium salt is likely to result in an increase of the hydrolysis-condensation kinetics, which is directly related to the viscosity of a sol and the thickness of a coating.

Table 2 Viscosities of Si–Zr hybrid sols doped with and without cerium salts.

Type	Viscosity (mPa·s)
Undoped	3.541 ± 0.121
$Ce(NO_3)_3$	4.217 ± 0.181
$CeCl_3$	4.357 ± 0.245
$Ce(CH_3COO)_3$	4.142 ± 0.316

3.2. Immersion tests

3.2.1. EIS analysis

Now we consider the evolution of EIS measurements with immersion time in 0.05 mol/L NaCl solution. The Bode plots of various hybrid coatings obtained after 1 h of immersion are presented in Fig. 2. As a comparison, the electrochemical behavior of the bare 2A12 aluminum alloy is also included in the Bode plots. It can be seen that all the samples with coatings show much higher impedance values at low frequencies than the bare 2A12 aluminum alloy, which means coatings can provide the aluminum alloy substrate with much better corrosion resistance. Except for that of bare 2A12, the phase plots show two well-defined time constants at the initial stage of immersion. The one at a high frequency (around 10^5 Hz) is attributed to the relaxation process of the external organic layer and the other time constant at a lower frequency results from the inorganic oxide layer between the metal surface and the hybrid coating. Compared with the other coatings, the coating doped with $Ce(CH_3COO)_3$ presents the highest phase angle between 10^3 and 10^5 Hz and the highest impedance value

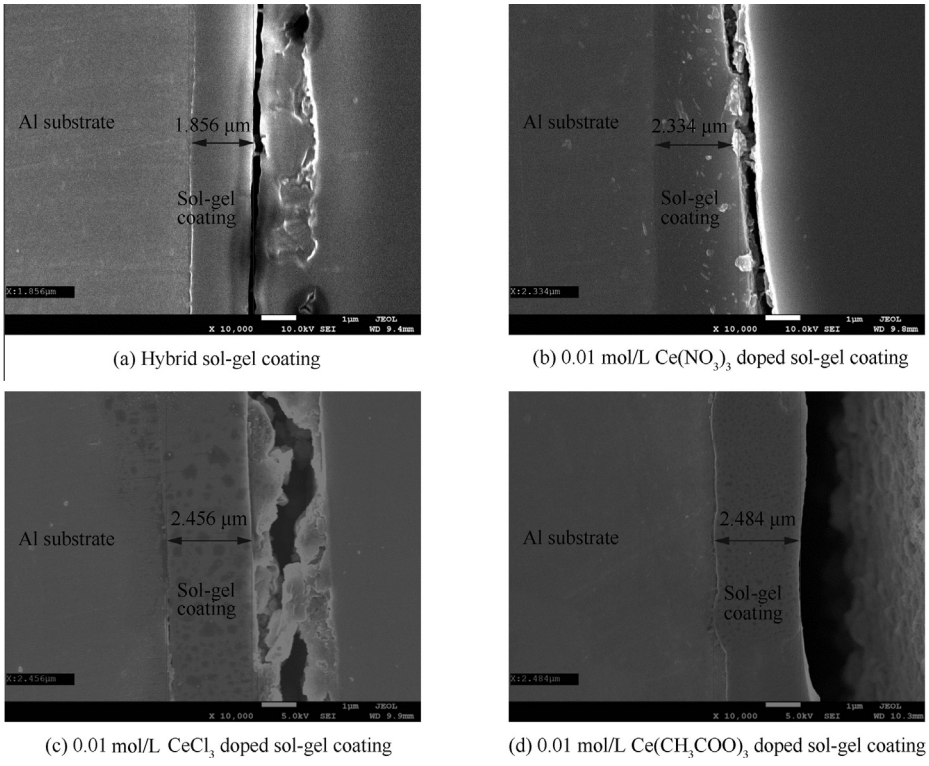

(a) Hybrid sol-gel coating

(b) 0.01 mol/L $Ce(NO_3)_3$ doped sol-gel coating

(c) 0.01 mol/L $CeCl_3$ doped sol-gel coating

(d) 0.01 mol/L $Ce(CH_3COO)_3$ doped sol-gel coating

Fig. 1 SEM images of the cross sections of various coatings.

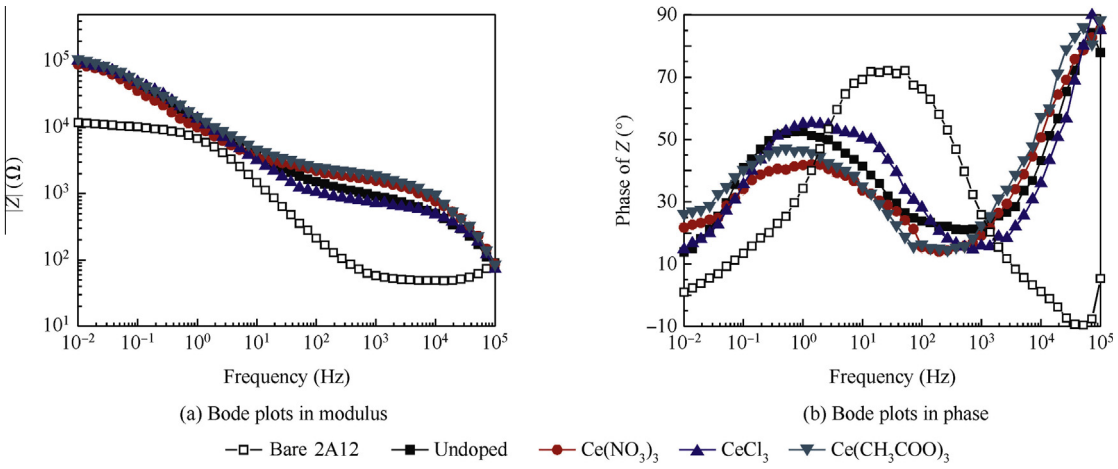

Fig. 2 Bode plots in modulus and phase of various coatings immersed in 0.05 mol/L NaCl solution for 1 h.

between 10^2 and 10^4 Hz, which shows that the $Ce(CH_3COO)_3$-doped coating has a better performance on the barrier properties of the external organic layer at the initial stage of immersion Figure 3 presents the Bode plots of various coatings after 24 h of immersion in 0.05 mol/L NaCl solution. It is observed that the resistance values of the coatings at low frequencies decrease significantly, especially for the coating doped with $CeCl_3$. This phenomenon is related to the role of Cl^-. There is extra Cl^- releasing from the $CeCl_3$-doped coating, which can accelerate the pitting corrosion on the substrate. The phase angles of the time constant at a high frequency decrease by about 10°, which indicates that electrolyte and water probably have penetrated through the organic layers and begin to attack the oxide layers. The phase angle of the time constant at a low frequency remarkably increases for the coating doped with $Ce(NO_3)_3$, which is likely due to the formation of oxides or hydroxides of cerium in the internal oxide layer.

The low-frequency impedance keeps on decreasing for the coating without an inhibitor after 72 h of immersion, while it increases in varying degrees for the coating doped with a cerium salt, which are shown in Fig. 4. The impedance of the coating doped with $Ce(CH_3COO)_3$ increases the most, followed by those with $Ce(NO_3)_3$ and $CeCl_3$. This increase of the impedance values reveals the self-healing effect of inhibitors by forming oxides of cerium on the corrosion spots,[32] and thus hindering the process of corrosion. For the $CeCl_3$-doped coating, Ce^{3+} and Cl^- would be simultaneously released from the hybrid coating to the substrate, so that the inhibition effect of Ce^{3+} and the demolishment of Cl^- on aluminum alloy would compete, resulting in a weaker corrosion resistance than the coatings doped with $Ce(NO_3)_3$ and $Ce(CH_3COO)_3$. The incorporation of $Ce(CH_3COO)_3$ makes the coating have significantly better barrier properties and higher stability against an electrolytic attack, which may be due to the synergistic effect provided by Ce^{3+} and CH_3COO^-. CH_3COO^- can participate in the formation of film by promoting the reactions of hydrolysis and condensation, which can be inferred later.

The Bode plots of various hybrid coatings after 168 h of immersion in 0.05 mol/L NaCl solution are shown in Fig. 5. It is clearly seen that the inhibited samples exhibit higher impedances when compared to the undoped one, and the coating doped with $Ce(CH_3COO)_3$ presents the highest impedance value. In addition, the phase angles of time constant at low frequencies increase remarkably for all coatings doped with cerium salts, indicating that oxides of cerium have been formed.

The quantitative interpretation of the EIS results for the undoped and Ce-doped hybrid coatings during the immersion period can be made by numerical fitting, and the applied equivalent electrical circuit models are depicted in Fig. 6. The

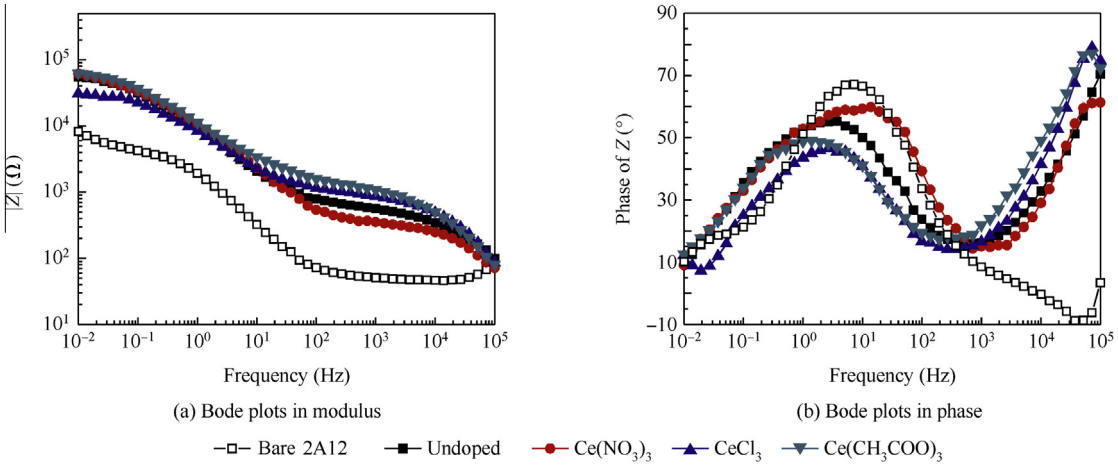

Fig. 3 Bode plots in modulus and phase of various coatings immersed in 0.05 mol/L NaCl solution for 24 h.

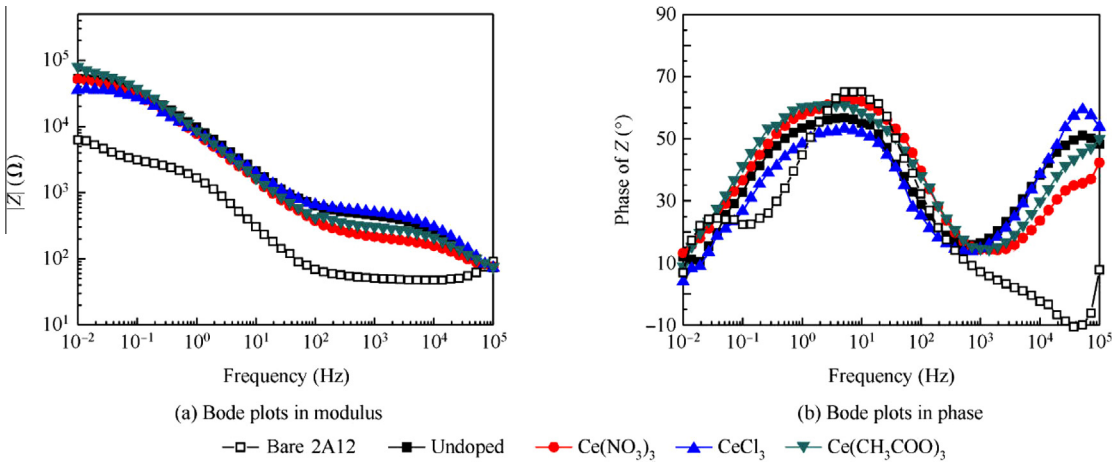

Fig. 4 Bode plots in modulus and phase of various coatings immersed in 0.05 mol/L NaCl solution for 72 h.

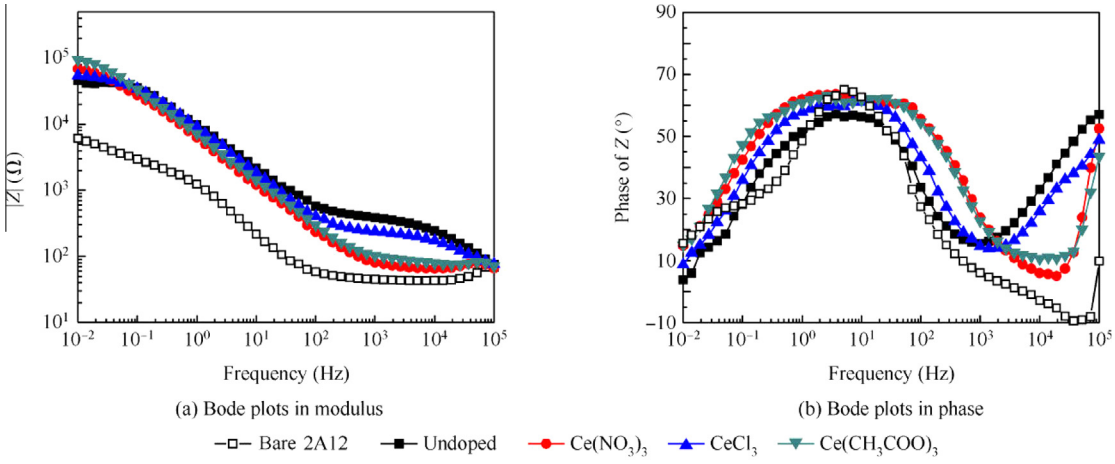

Fig. 5 Bode plots in modulus and phase of various coatings immersed in 0.05 mol/L NaCl solution for 168 h.

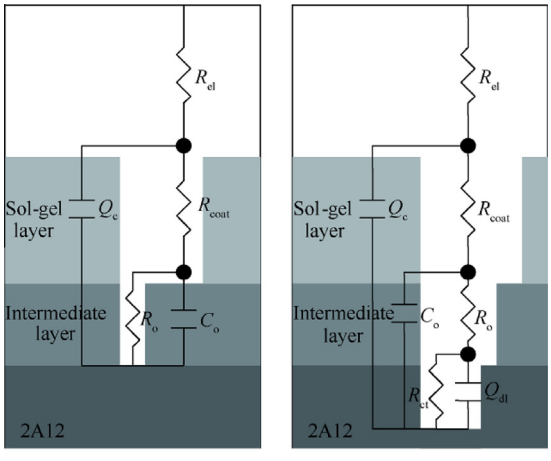

Fig. 6 Equivalent circuits used for numerical fitting of the EIS data.

equivalent circuit in Fig. 6(a) is used for the coatings without signs of corrosion on the aluminum substrate at the initial stage of immersion; the circuit in Fig. 6(b) is used for the coatings after longer immersion. In the circuits, R_{el} is the resistance of the solution, and Q_c and R_{coat} are the capacitance and resistance of the sol–gel coating, while C_o and R_o are the capacitance and resistance of the inorganic oxide layer between the metal surface and the coating. After corrosion occurred on the aluminum substrate, another panel of elements, Q_{dl} and R_{ct}, are added and represent the capacitance of the double layer and the resistance of the charge transfer process, respectively. As an example, Fig. 7 shows the fitted results for the undoped coating, which are in good agreement with the experimental data.

The evolutions of R_{coat} and R_o values of the four coatings during continuous immersion are shown in Fig. 8. R_{coat} decreases with immersion time. However, a slight increase of R_{coat} values after 24 h of immersion can be observed for the coating doped with $CeCl_3$, which may be ascribed to the blocking effect of cerium oxide in the pinholes of the coating. The oxide layer is the last barrier to prevent the substrate from being attacked by corrosive agents and water. Undoubtedly, all

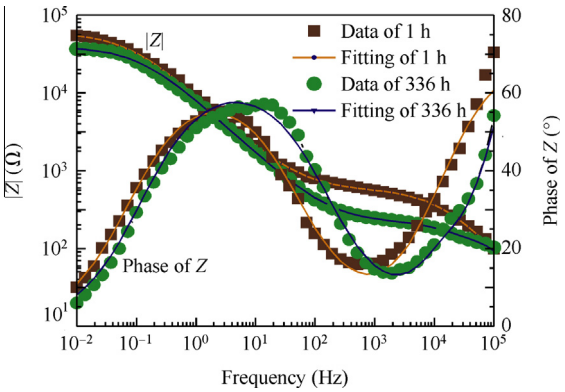

Fig. 7 Fitted EIS spectrum for the undoped coating after immersion.

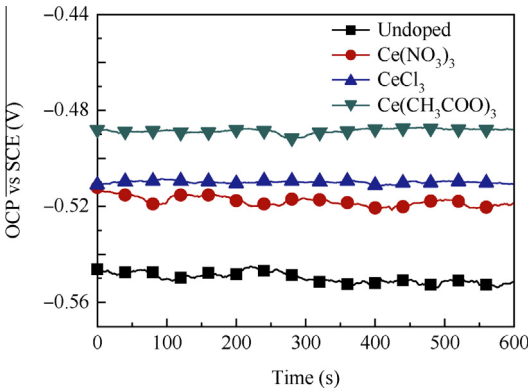

Fig. 9 OCP vs SCE recorded before the acquisition of EIS spectra after 168 h of immersion.

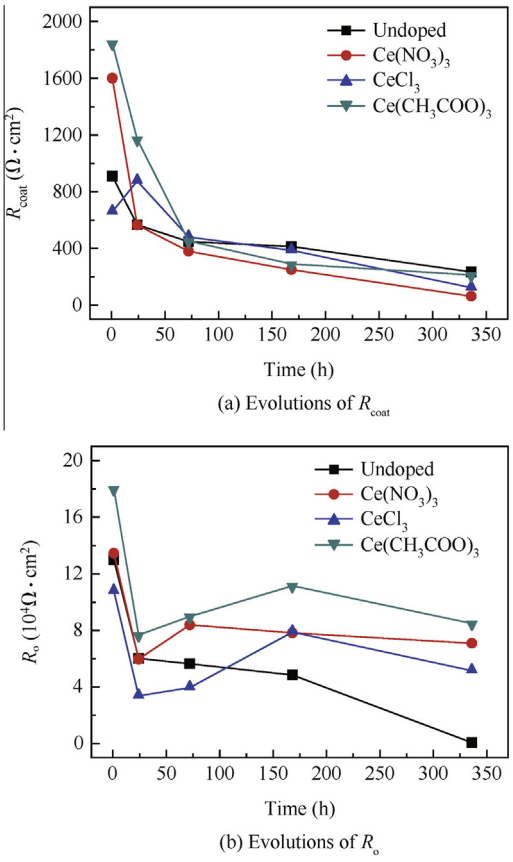

Fig. 8 Evolutions of R_{coat} and R_o for various coatings during immersion in 0.05 mol/L NaCl solution.

values of resistance of oxide layers R_o decrease with time at the initial stage of immersion (1–24 h), which is due to the water uptake. According to Refs.[33,34] the oxide layer between a hybrid coating and a metal substrate is basically composed of metal–O–Si covalent bonds, namely Al–O–Si and Al–O–Zr bonds in the present work. From Fig. 8(b), it can also be seen that the coating doped with $Ce(CH_3COO)_3$ exhibits the highest R_o during most time of immersion, indicating that the addition of $Ce(CH_3COO)_3$ increases the Al–O–Si/Zr bond density across the substrate/coating interface and enhances the compactness of the resulted oxide layer. For the coatings doped with cerium salts, R_o increases with immersion time in varying degrees, indicating that the oxides or hydroxides of cerium are stably formed with the release of Ce from the hybrid coating.

3.2.2. OCP analysis

As a supplementary instruction, OCPs obtained after 168 h of immersion are shown in Fig. 9. The exposed area of all the samples for the OCP corrosion tests was 1 cm^2. Under the experimental condition, it can be observed that the OCPs of the Ce-doped samples are always higher than that of the undoped one. Additionally, the coating doped with $Ce(CH_3COO)_3$ possesses the most positive OCP values. In spite of the fact that the OCP values cannot provide any direct information about the corrosion kinetics, the increase of OCP for the Ce-doped coatings suggests the reduction of susceptibility of the coatings to the corrosion process due to the presence of inhibitors.

3.2.3. Surface morphologies after immersion

The typical morphologies of the hybrid coatings after 25 days of immersion in 0.05 M NaCl solution are shown in Fig. 10. There are amount of corrosion products accumulating on the undoped coating, as shown in Fig. 10(a). It indicates that the coating without an inhibitor doped cannot provide an effective protection in long-time immersion. On the contrary, the coatings doped with cerium salts exhibit improved corrosion protection ability, as shown in Figs. 10(b)–(d). From Fig. 10(b), it can be seen that the surface morphology of the $Ce(NO_3)_3$-doped coating is relatively smooth. The magnified image reveals that cracking has happened due to internal stress at the local area. For the $CeCl_3$-doped coating (Fig. 10(c)), typical pitting morphology can be found. By comparison, the coating doped with $Ce(CH_3COO)_3$ (Fig. 10(d)) appears to be pristine and crack-free, and few enlarged pores are observed on the surface, which indicates that CH_3COO^- can inhibit the corrosion process of the substrate effectively and achieve a stronger corrosion resistance.

3.3. Salt spray tests

The neutral salt spray test was applied to evaluate the corrosion resistance of the coated 2A12 aluminum substrates in severe environment. The optical images of four coatings after 96 h exposure in a 5 wt% NaCl neutral salt spray chamber are shown

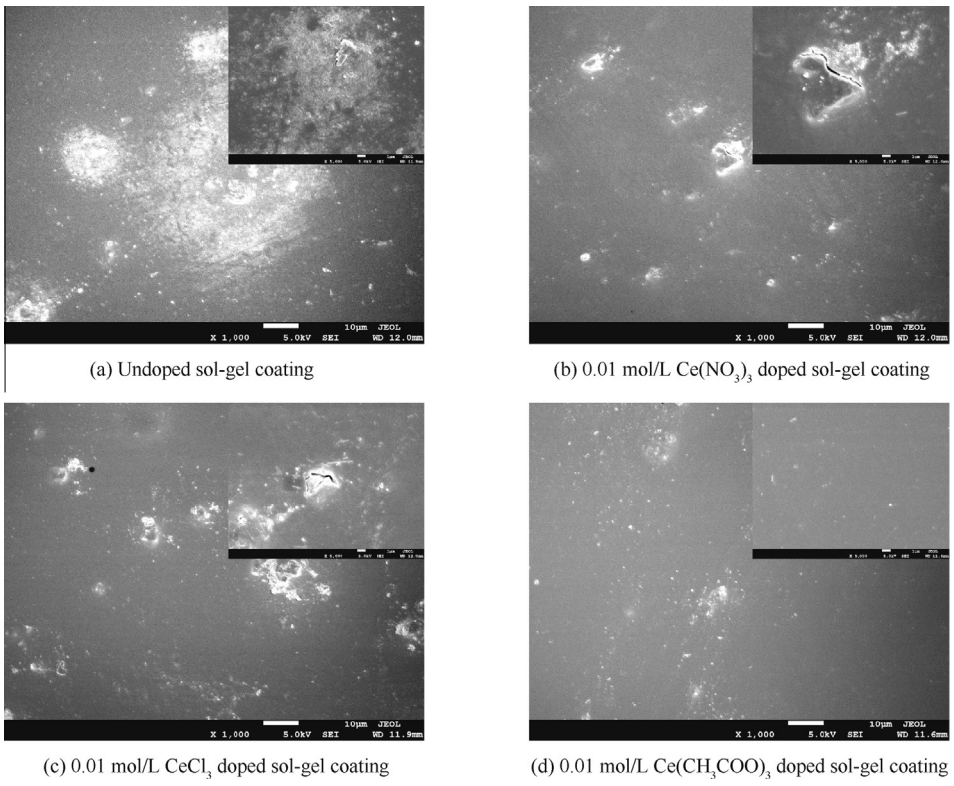

(a) Undoped sol-gel coating

(b) 0.01 mol/L $Ce(NO_3)_3$ doped sol-gel coating

(c) 0.01 mol/L $CeCl_3$ doped sol-gel coating

(d) 0.01 mol/L $Ce(CH_3COO)_3$ doped sol-gel coating

Fig. 10 Surface morphologies of various coatings after 25 days of immersion in 0.05 mol/L NaCl.

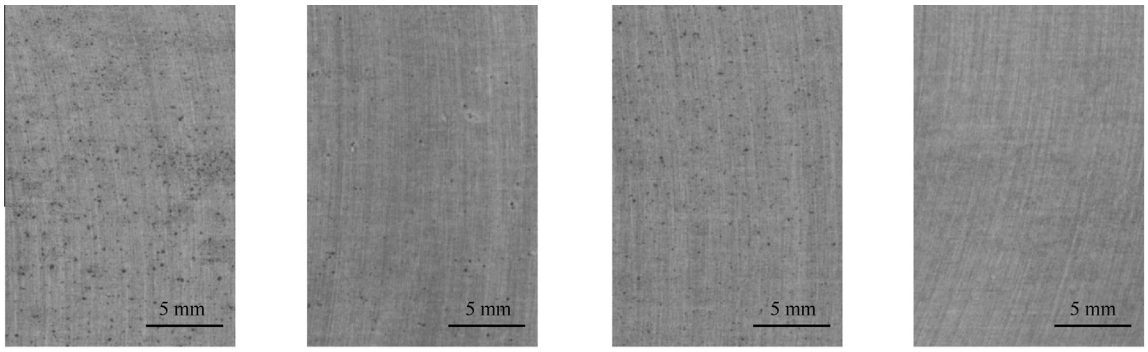

(a) Undoped sol-gel coating

(b) 0.01 mol/L $Ce(NO_3)_3$ doped sol-gel coating

(c) 0.01 mol/L $CeCl_3$ doped sol-gel coating

(d) 0.01 mol/L $Ce(CH_3COO)_3$ doped sol-gel coating

Fig. 11 Photos of various coatings after 96 h exposure in a salt-spray chamber.

in Fig. 11. The undoped coating in Fig. 11(a) is badly damaged, with a large number of pitting sites across the surface. Tiny pitting corrosion is also observed for the coating doped with 0.01 M $CeCl_3$ in Fig. 11(c). As expected, no pitting is detected on the surface of the coating doped with $Ce(CH_3COO)_3$ in Fig. 11(d). In short, the Ce-doped coatings exhibit improved corrosion protection after 96 h exposure in the neutral salt spray chamber, which is in agreement with the results of immersion tests.

3.4. FTIR analysis

The FTIR transmittance spectra for various coatings deposited on 2A12 samples are shown in Fig. 12. To get a full and detailed vision, the spectra were broken at 1800 cm^{-1} and divided into two parts with different wavenumber increments.

For all the hybrid coatings, two noticeable peaks at 1084 cm^{-1} and 1052 cm^{-1} are assigned to Si–O–Si stretching vibration in cage and network configurations formed by the condensation reaction of silanol.[35,36] Small peaks observed at around 952 cm^{-1} correspond to the Si–O–Zr bonds.[37] It is concluded that a hybrid network containing zirconia and organo-silica is formed in the sol–gel coatings.

The peak around 1275 cm^{-1} is attributed to the vibration of epoxy groups.[33] The intensity of this peak for the coating doped with $Ce(NO_3)_3$ is significantly high, indicating that no ring-opening reaction has happened during the deposition of glycidoxypropyl-trimethoxy-silane (GTMS). In this case, it is

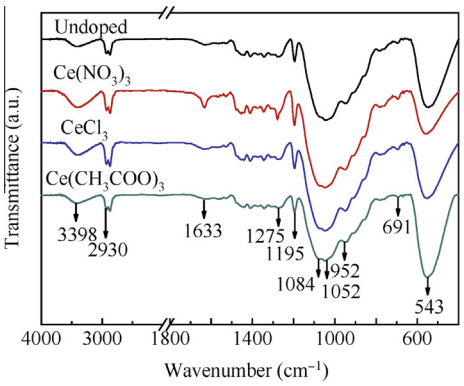

Fig. 12 Infrared spectra of various coatings.

beneficial for the deposition of epoxy silane on the aluminum alloy substrate. The existence of an epoxy group can increase the flexibility and hydrophobicity of the coating, and consequently improve the protective performance. The coating doped with $Ce(CH_3COO)_3$ presents the highest intensity at 543 cm^{-1}, which is due to C–H out-of-plane deformation of the aromatic ring of epoxy resin.[38] The result indicates that $Ce(CH_3COO)_3$ is in favor of ring-opening reaction and thus forms a dense three-dimensional network structure. The peaks around 1195 cm^{-1} and 3398 cm^{-1} are assigned to Si–O–CH_3 and Si–OH vibrations, respectively, and the peak intensities of the coatings doped with $Ce(NO_3)_3$ and $CeCl_3$ are obviously higher than that of the $Ce(CH_3COO)_3$-doped coating. It indicates that the reactant of hydrolysis (Si–O–CH_3 bond) and the reactant of condensation (Si–OH bond)[39] in the inorganic cerium-doped sols do not react completely, while $Ce(CH_3COO)_3$ can promote the reactions of hydrolysis and condensation. The results mentioned above show that the addition of cerium salt inhibitors can still get stabilized Si–Zr organic–inorganic hybrid coatings. $Ce(NO_3)_3$ is in favor of the deposition of epoxy silane on the aluminum alloy substrate. $Ce(CH_3COO)_3$ can promote the reactions of hydrolysis and condensation, as well as the formation of a dense three-dimensional network structure. The above conclusion explains the reason of an increased Al–O–Si/Zr bond density (refer to Fig. 8), and provides a possible interpretation of the better corrosion performance for $Ce(CH_3COO)_3$-doped coatings.

4. Conclusions

The effects of various cerium salts on the structure, morphology, and corrosion resistance of Si–Zr hybrid coatings were investigated. The results show that addition of 0.01 mol/L cerium salts hinders the process of corrosion by forming oxides of cerium on corrosion spots, and thus significantly improves the corrosion resistance of hybrid coatings. For $CeCl_3$-doped coatings, Ce^{3+} and Cl^- would be simultaneously released from the hybrid coating to the substrate, so that the inhibition effect of Ce^{3+} and the demolishment of Cl^- on aluminum alloy would compete, resulting in a weaker corrosion protection than coatings doped with other cerium salts. The incorporation of $Ce(CH_3COO)_3$ makes a coating have significantly better barrier properties and higher stability against electrolytic attacks. Thereinto, CH_3COO^- can participate in the formation of a coating by promoting the reactions of hydrolysis and condensation, and thus effectively increase the Al–O–Si/Zr bond density and improve the compactness of the resulted coating. The above conclusion provides a possible interpretation of the better corrosion performance for $Ce(CH_3COO)_3$-doped coatings.

Acknowledgments

This work was supported by the National Natural Science Foundation of China (No. 21371019) and the Aeronautical Science Foundation of China (No. 2011ZE51057).

References

1. Starke EA, Staley JT. Application of modern aluminum alloys to aircraft. *Prog Aerospace Sci* 1996;**32**(2):131–72.
2. Voevodin N, Jeffcoate C, Simon L, Khobaib M, Donley M. Characterization of pitting corrosion in bare and sol-gel coated aluminum 2024-T3 alloy. *Surf Coat Technol* 2001;**140**(1):29–34.
3. Feng Z, Liu Y, Hashimoto T, Thompson GE, Zhou X, Skeldon P. Influence of surface pretreatments on the corrosion protection of sol-gel coated AA2024-T3 aluminium alloy. *Surf Interface Anal* 2013;**45**(10):1452–6.
4. Ding JJ, Li SM, Liu JH, Yu M, Zhan ZW. Cobaltous acetate doped sol-gel coatings for corrosion protection on aluminium alloy LY12. *Acta Aeronautica et Astronaut Sin* 2011;**32**(6):1147–55.
5. Akid R, Gobara M, Wang H. Corrosion protection performance of novel hybrid polyaniline/sol-gel coatings on an aluminium 2024 alloy in neutral, alkaline and acidic solutions. *Electrochim Acta* 2011;**56**(5):2483–92.
6. Huang JF. *The principle and technology of sol–gel*. Beijing: Chemical Industry Press; 2005, p. 138–43 [Chinese].
7. Liu JH, Dong L, Yu M, Li SM, Zhan ZW. Preparation and properties of silicon-zirconium hybrid coatings by electrophoretic deposition on LC4 aluminum alloy. *Acta Chim Sinica* 2012;**70**(20):2179–86.
8. Fu CJ, Zhan ZW, Yu M, Li SM, Liu JH, Dong L. Influence of Zr/Si molar ratio on structure, morphology and corrosion resistance of organosilane coatings doped with zirconium(IV) *n*-propoxide. *Int J Electrochem Sci* 2014;**9**:2603–19.
9. Wang D, Bierwagen GP. Sol-gel coatings on metals for corrosion protection. *Prog Org Coat* 2009;**64**(4):327–38.
10. Feng Z, Liu Y, Thompson GE, Skeldon P. Sol-gel coatings for corrosion protection of 1050 aluminium alloy. *Electrochim Acta* 2010;**55**(10):3518–27.
11. Metroke TL, Kachurina O, Knobbe ET. Spectroscopic and corrosion resistance characterization of GLYMO-TEOS Ormosil coatings for aluminum alloy corrosion inhibition. *Prog Org Coat* 2002;**44**(4):295–305.
12. Brusciotti F, Batan A, Graeve ID, Wenkin M, Biessemans M, Willem R, et al. Characterization of thin water-based silane pretreatments on aluminium with the incorporation of nano-dispersed CeO_2 particles. *Surf Coat Technol* 2010;**205**(2):603–13.
13. Matter EA, Kozhukharov S, Machkova M, Kozhukharov V. Comparison between the inhibition efficiencies of Ce(III) and Ce(IV) ammonium nitrates against corrosion of AA2024 aluminum alloy in solutions of low chloride concentration. *Corros Sci* 2012;**62**:22–33.
14. Peng SS, Zhao WJ, Zeng ZX, Li H, Xue QJ, Wu XD. Preparation of anticorrosion hybrid silica sol-gel coating using $Ce(NO_3)_3$ as catalyst. *J Sol-Gel Sci Technol* 2013;**66**(1):133–8.
15. Lakshmi RV, Yoganandan G, Kavya KT, Basu BJ. Effective corrosion inhibition performance of Ce^{3+} doped sol-gel nanocomposite coating on aluminum alloy. *Prog Org Coat* 2013;**76**(2):367–74.

16. Tedim J, Zheludkevich ML, Bastos AC, Salak AN, Lisenkov AD, Ferreira MGS. Influence of preparation conditions of layered double hydroxide conversion films on corrosion protection. *Electrochim Acta* 2014;**117**:164–71.
17. Hinton BRW. Corrosion inhibition with rare earth metal salts. *J Alloys Compd* 1992;**180**(1):15–25.
18. Aldykiewicz Jr AJ, Davenport AJ, Isaacs HS. Studies of formation of cerium-rich protective films using X-ray absorption near-edge spectroscopy and rotating disk electrode methods. *J Electrochem Soc* 1996;**143**(1):147–54.
19. Irfan A, Zhang Q, Xiang M. Corrosion inhibition of SiC_p/5A06 aluminum metal matrix composite by cerium conversion treatment. *Chin J Aeronaut* 2009;**22**(6):670–6.
20. Raps D, Hack T, Wehr J, Zheludkevich ML, Bastos AC, Ferreira MGS, et al. Electrochemical study of inhibitor-containing organic-inorganic hybrid coatings on AA2024. *Corros Sci* 2009;**51**(5):1012–21.
21. Zheludkevich ML, Poznyak SK, Rodrigues LM, Raps D, Hack T, Dick LF, et al. Active protection coatings with layered double hydroxide nanocontainers of corrosion inhibitor. *Corros Sci* 2010;**52**(2):602–11.
22. Tavandashti NP, Sanjabi S. Corrosion study of hybrid sol-gel coatings containing boehmite nanoparticles loaded with cerium nitrate corrosion inhibitor. *Prog Org Coat* 2010;**69**(4):384–91.
23. Yasakau KA, Kallip S, Zheludkevich ML, Ferreira MGS. Active corrosion protection of AA2024 by sol-gel coatings with cerium molybdate nanowires. *Electrochim Acta* 2013;**112**:236–46.
24. Mishra AK, Balasubramaniam R. Corrosion inhibition of aluminum alloy AA 2014 by rare earth chlorides. *Corros Sci* 2007;**49**(3):1027–44.
25. Montemor MF, Ferreira MGS. Electrochemical study of modified bis-triethoxysilylpropyl tetrasulfide silane films applied on the AZ31 Mg alloy. *Electrochim Acta* 2007;**52**(27):7486–95.
26. Yurt A, Bereket G, Ogretir C. Quantum chemical studies on inhibition effect of amino acids and hydroxy carboxylic acids on pitting corrosion of aluminium alloy 7075 in NaCl solution. *J Mol Struct Theochem* 2005;**725**(1):215–21.
27. Bereket G, Yurt A. The inhibition effect of amino acids and hydroxy carboxylic acids on pitting corrosion of aluminium alloy 7075. *Corros Sci* 2001;**43**(6):1179–95.
28. Markley TA, Forsyth M, Hughes AE. Corrosion protection of AA2024-T3 using rare earth diphenyl phosphates. *Electrochim Acta* 2007;**52**(12):4024–31.
29. Shi HW, Han EH, Liu FC. Corrosion protection of aluminium alloy 2024-T3 in 0.05 M NaCl by cerium cinnamate. *Corros Sci* 2011;**53**(7):2374–84.
30. White PA, Hughes AE, Furman SA, Sherman N, Corrigan PA, Glenn MA, et al. High-throughput channel arrays for inhibitor testing: Proof of concept for AA2024-T3. *Corros Sci* 2009;**51**(10):2279–90.
31. Paussa L, Navarro NCR, Bravin D, Andreatta F, Lanzutti A, Aparicio M, et al. ZrO_2 sol-gel pretreatments doped with cerium nitrate for the corrosion protection of AA6060. *Prog Org Coat* 2012;**74**(2):311–9.
32. Shi HW, Liu FC, Han EH. Corrosion behaviour of sol-gel coatings doped with cerium salts on 2024-T3 aluminum alloy. *Mater Chem Phys* 2010;**124**(1):291–7.
33. Kim J, Wong PC, Wong KC, Sodhi RNS, Mitchell KAR. Adsorption of BTSE and γ-GPS organosilanes on different microstructural regions of 7075-T6 aluminum alloy. *Appl Surf Sci* 2007;**253**(6):3133–43.
34. Quinton JS, Dastoor PC. Characterizing the bonding mechanisms at silane-metal interfaces: a model system. *J Mater Sci Lett* 1999;**18**(22):1833–5.
35. Oliver MS, Blohowiak KY, Dauskardt RH. Molecular structure and fracture properties of ZrO_X/Epoxysilane hybrid films. *J Sol-Gel Sci Technol* 2010;**55**(3):360–8.
36. Park ES, Ro HW, Nguyen CV, Jaffe RL, Yoon DY. Infrared spectroscopy study of microstructures of poly(silsesquioxane)s. *Chem Mater* 2008;**20**(4):1548–54.
37. Armelao L, Gross S, Müller K, Pace G, Tondello E, Tsetsgee O, et al. Structural evolution upon thermal heating of nanostructured inorganic-organic hybrid materials to binary oxides MO_2–SiO_2 (M = Hf, Zr) as evaluated by solid-state NMR and FTIR spectroscopy. *Chem Mater* 2006;**18**(25):6019–30.
38. Kartsonakis IA, Koumoulos EP, Balaskas AC, Pappas GS, Charitidis CA, Kordas GC. Hybrid organic-inorganic multilayer coatings including nanocontainers for corrosion protection of metal alloys. *Corros Sci* 2012;**57**:56–66.
39. Deepa PN, Kanungo M, Claycomb G, Sherwood PMA, Collinson MM. Electrochemically deposited sol-gel-derived silicate films as a viable alternative in thin-film design. *Anal Chem* 2003;**75**(20):5399–405.

Yu Mei received her Ph.D. degree from Beihang University in 2007 and is now an associate professor of materials science and engineering at the same university. Her main research interests are nano functional materials, corrosion science and protection technology.

Liu Yuxing received her B.S. degree from Chongqing University in 2012 and M.S. degree from Beihang University. Her main research interests are corrosion science and protection technology.